Supporting Information

Huber et al. 10.1073/pnas.1700328114

SI Methods

Generation of Expression Constructs. DNA fragments of *Homo sapiens* DPF2 were amplified by PCR and cloned into the vector pGEX-6P-1 (GE Healthcare) and the lentiviral expression vector CDH-EF1-MCS-(PGK-GFP) (System Biosciences). DPF2 mutants were generated by QuikChange mutagenesis (Stratagene) and confirmed by DNA sequencing. Viruses were produced by transfection of 293T cells with vectors, according to standard protocols (1). Details of all constructs are listed in Tables S1 and S4.

Recombinant Protein Expression and Purification. All proteins were expressed in *Escherichia coli* BL21-CodonPlus(DE3)-RIL cells (Stratagene) grown in LB media supplemented with 0.1 mM zinc acetate and appropriate antibiotics. Protein expression was induced at an OD_{600} of ∼0.6 with 0.5 mM isopropyl β-D-thiogalactoside (IPTG) for 18 h at 18 °C. Cells were harvested by centrifugation and resuspended in a buffer containing 20 mM Tris (pH 8.0), 100 mM NaCl, 5 mM DTT, 2 μM bovine lung aprotinin (Sigma), and complete EDTA-free protease inhibitor mixture (Roche), and subsequently flash-frozen in liquid nitrogen. Thawed cells were lysed with a cell disrupter (Avestin) and the lysate was centrifuged for 1 h at 40,000 × *g*. The cleared lysate was applied to a glutathione Sepharose column (GE Healthcare) equilibrated in buffer containing 20 mM Tris (pH 8.0), 100 mM NaCl, and 5 mM DTT, and eluted via a glutathione gradient. Pooled fractions were cleaved with PreScission protease (GE Healthcare) for 12 h. Cleaved protein was bound to a HiTrapQ HP (GE Healthcare) column and eluted via a linear NaCl gradient, concentrated, and injected onto a HiLoad 16/60 Superdex 75 column equilibrated in 20 mM Tris (pH 8.0), 100 mM NaCl, and 5 mM DTT. Pooled fractions were concentrated to 15 mg/mL and used in subsequent crystallization trials or for in vitro binding assays.

Structure Determination and Refinement. Crystals of $DPF2^{PHD}$ were grown at 21 °C in hanging drops containing 1 μL of the protein and 1 μL of a reservoir solution consisting of 2.2 M ammonium sulfate and 0.15 M ammonium citrate. Crystals grew in the tetragonal space group *I*422 and reached a maximum size of ∼500 μm × 500 μm × 500 μm within a week. For cryoprotection, crystals were stabilized in the crystallization solution supplemented with 20% (vol/vol) ethylene glycol (added in 5% increments). X-ray diffraction data were collected at 100 K at beamline 12–2 at the Stanford Synchrotron Radiation Lightsource (SSRL). X-ray intensities were processed using XDS (2). The structure was solved by single-wavelength anomalous dispersion using X-ray diffraction data collected using the anomalous scattering of the endogenous Zn^{2+} ions. Identification of heavy metal sites, calculation of phases, and density modification were performed in PHENIX (3). Iterative rounds of model building and refinement in Coot and PHENIX yielded final models containing all residues of $DPF2^{PHD}$ fragment, except for residues 387–391, for which no electron density was observed (3, 4). The final R_{work} and R_{free} values were 14.6% and 18.7%, respectively. The model possesses excellent stereochemical parameters with no residues in the disallowed regions of the Ramachandran plot as assessed with MolProbity (5). For details of the data collection and refinement statistics, see Table S2.

CD Spectroscopy. Purified DPF2 wild-type and triple mutant protein ($DPF2^{MUT}$) was dialyzed into buffer containing 20 mM sodium phosphate (pH 8.0) and 1 mM DTT and concentrated to ∼15 mg/mL. CD spectra were measured with a Circular Dichroism Spectrometer Model 430 (Aviv Biomedical) in triplicate. Data were collected at protein concentrations of 0.25 mg/mL at 25 °C in 1-nm increments and an averaging time of 5 s.

ITC Measurements. ITC measurements were performed at 25 °C using a MicroCal ITC200 Calorimeter (Malvern). Protein samples were stored in a buffer containing 25 mM HEPES (pH 8.0), 100 mM NaCl, 2 mM tris(2-carboxyethyl)phosphine (TCEP), and 10% (vol/vol) glycerol. The lyophilized H3 and H4 peptide variants were dissolved in buffer containing 25 mM HEPES (pH 8.0), 2 mM TCEP, and 10% (vol/vol) glycerol to generate 100-mM stock solutions. For measurements at 50 mM NaCl or 100 mM NaCl concentrations, these peptide stock solutions were diluted accordingly. All measurements were performed in triplicate. The heat generated from dilution was subtracted for baseline correction. Baseline corrected data were analyzed with Origin 7.0 software.

Purification, Infection, and Culture of HSPC $CD34^+$ Cells. $CD34^+$ HSPCs were purified by positive selection using the Midi MACS (magnetic-activated cell sorting) LS^+ separation columns and isolation kit (Miltenyi) starting with mononuclear cells that were isolated from CB by Ficoll-Hypaque Plus (GE Healthcare Life Sciences) density centrifugation. $CD34^+$ cells were cultured in Iscove's modified Dulbecco's medium (Cellgro) 20% BIT 9500 medium (StemCell Technologies) supplemented with SCF (100 ng/mL), FLT-3 ligand (10 ng/mL), IL-6 (20 ng/mL), and TPO (100 ng/mL) as the basic culture. $CD34^+$ cells were infected with high-titer lentiviral concentrated suspensions, with 8 μg/mL polybrene (Sigma-Aldrich). To differentiate HSPCs, cells were cultured under the myeloid-promoting conditions: SCF (100 ng/mL), FLT-3 ligands (10 ng/mL), IL-3 (20 ng/mL), IL-6 (20 ng/mL), GM-CSF (20 ng/mL), and G-CSF (20 ng/mL) (all purchased from Peprotech).

Cell Fractionation. Cellular fractions from 293T cells were obtained using the Subcellular Protein Fractionation Kit for Cultured Cells (ThermoFisher Scientific). The following antibodies were used to distinguish the individual fractions: for the cytoplasmic fraction, Caspase-3 (9665, Cell Signaling); nuclear soluble fraction, Sp-1 (sc-59, Santa Cruz); and chromatin bound fraction, Lamin B (sc-6216). FLAG-DPF2 was detected using anti-FLAG M2-HRP (A8592, Sigma Aldrich).

Mass Spectrometry of DPF2 Interacting Proteins. To precipitate endogenous DPF2, 200 μL of protein A/G magnetic beads (88803, Thermo Scientific) were cross-linked to 20 μg of the polyclonal rabbit anti-DPF2 antibody (A303-595A, Bethyl Laboratories) using dimethyl pimelimidate dihydrochloride (D8388, Sigma-Aldrich). Lysates from SKNO-1 and Kasumi-1 cells were incubated with 5 μg of anti-DPF2 conjugated beads and eluted with 50 μL of 1 M glycine (pH 3.0). Proteins were precipitated using the Proteoextract Protein Precipitation Kit (539180, EMD Millipore) and submitted for mass spectrometry analysis as a dry pellet. The following antibodies were used for the confirmation of SWI/SNF complex interactions with endogenous and FLAG tagged DPF2: BAF155 (11956, Cell Signaling), SMARCC2 (12760, Cell Signaling), and ACTL6A (ab131272, Abcam).

Immunofluorescence Microscopy. The 293T cells transfected with pCDNA3.1-FLAG vector harboring wild-type or mutant FLAG-DPF2 plasmids were grown on coverslips overnight. Cells were

fixed with 4% (wt/vol) PFA for 10 min in DMEM supplemented with 10% (vol/vol) FBS and permeabilized for 10 min with PBS supplemented with 0.25% (vol/vol) Triton-X. Following blocking in PBST for 1 h, cells were incubated with anti-FLAG antibody conjugated to FITC (F4049, Sigma-Aldrich) at 1:300 overnight. Slides were imaged using the Leica SP5 inverted confocal microscope.

Immunoprecipitation of FLAG-Tagged Constructs. The 293T cells were transfected with pCDNA3.1-FLAG vector harboring FLAG-DPF2 wild-type and FLAG-DPF2^{MUT}. Immunoprecipitation for FLAG-DPF2 was conducted overnight by incubating 500 μg of cell lysate with 20 μL of anti-FLAG M2 Magnetic beads (M8823, Sigma-Aldrich). For histone acetylation assays, cells were incubated with 1 μM of histone deacetylase inhibitor, Vorinostat (SAHA, MK0683, Selleckchem), or DMSO for 24 h. Antibodies used for Western blot were anti-H3 (sc-8654, Santa-Cruz), anti-H4 (ab17036, Abcam), or anti-FLAG M2 (F1084, Sigma Aldrich). For the immunoprecipitation of FLAG-RUNX1, a total of 200,000 HEL cells were infected for 16 h with concentrated lentiviral particles (25 multiplicity of infection) and 4 μg/mL polybrene (Sigma Aldrich). After 24 h, cells were infected for 16 h with DPF2 or DPF2^{PHD} lentiviral particles at a multiplicity of infection of 10 and 4 μg/mL polybrene. After 72 h cells were lysed in nuclei extraction buffer and FLAG-RUNX1 was immunoprecipitated with anti-FLAG magnetic beads as indicated above. DPF2 and DPF2^{PHD} proteins were detected using anti-DPF2 at a concentration of 1:1,000 (ab74519, Abcam). Virally expressed DPF2 and DPF2^{PHD} were overexpressed 100-fold in HEL cells compared with endogenous DPF2.

Generation of Lentivirus. Wild-type, triple mutant, and a region encompassing the tandem PHD domain of DPF2 were cloned into the pCDH-EF1-MCS-(PGK-GFP) lentiviral expression Vector (System Biosciences). Viruses were produced by transfection of 5 million human embryonic kidney 293T cells with 10 μg of plasmid, using the Calcium Phosphate Transfection Kit (Invitrogen) with helper plasmids (3.5 μg psPAX2 and 7.5 μg pMD2.G), according to standard protocols (1). Both helper plasmids were a gift from Didier Trono (School of Life Sciences, École Polytechnique Fédérale de Lausanne (EPFL), Lausanne, Switzerland; Addgene plasmid #12260 and #12259). Details of all lentiviral constructs are listed in Table S4.

Immunoblot Analysis. Cells were harvested, counted, and washed with PBS and lysed in cell lysis buffer (Cell Signaling) supplemented with protease and phosphatase inhibitors. Lysates were resolved on 4–12% gradient SDS-PAGE gels and transferred to 0.2-μm nitrocellulose membranes (Bio-Rad). Membranes were blocked with 5% blotting grade blocker (Bio-Rad) and probed using DPF2 (S-24) (sc-101943; Santa Cruz) and β-actin (N-21) (sc-130656; Santa Cruz). For recognition of full-length DPF2 and DPF2^{PHD}, anti-DPF2 antibody was used (ab74519, Abcam).

Flow Cytometry. CD34 cells were isolated from umbilical CB and transduced with a lentivirus expressing the pCDH-EF1-MCS-(PGK-GFP) vector alone, wild-type DPF2, or DPF2^{MUT}. Cells were cultured for 7 d in X-vivo media supplemented with 20% BIT and myeloid differentiation promoting cytokines (IL-3, IL-6, SCF, and GM-CSF). Transduced CD34^{+} cells were stained with CD11b-PE (BD Pharmingen) and analyzed on a BD FACSCanto flow cytometer. Infected cells were selected by gating those expressing GFP and examined for changes in CD11b positivity using the FloJo analysis software.

RNA-Sequencing and Data Analysis. Human primary CD34^{+} cells were purified from umbilical CB using Ficoll separation followed by magnetic enrichment for CD34^{+} cells using the CD34 microbead purification kit (Miltenyl Biotech). Lentivirus particles encoding DPF2 shRNA or a scrambled control were produced in 293T cells and concentrated using the retro-x concentrator (Clontech). Cells were infected with lentivirus by spin infection and harvested 3 d postinfection. Cells positive for the lentiviral infection were sorted based on GFP positivity using a fluorescent activated cell sorter. Total RNA was extracted from the sorted cells using the RNeasy mini kit (Qiagen). RNA-Seq library prep was carried out using the Illumina TruSeq Total Stranded kit (RS-122-2201) with Ribo-Zero rRNA reduction following manufacturer's standard protocol without modification. Next, 500 ng of total RNA was used as input with RNA quality assessed using Agilent Bioanalyzer 2100 Nano 6000. Library quantification and balancing was done using Kapa Biosciences Library Quantification (Complete, K4824) run on a Roche LC480 LightCycler. Samples were loaded in a single 300 cycles High Output NextSEq. 500 V1 flow cell (FC-404-1004) per manufacturer's standard protocol. Experiments were performed in triplicate. Data analysis was performed using the Illumina BaseSpace platform (https://basespace.illumina.com/home/index) for base-calling and demultiplexing.

ChIP Assays. Approximately 4 × 10^{6} cells were used per ChIP reaction after cross-linking with 1% (wt/vol) formaldehyde for 10 min at room temperature. ChIP assays were performed using ChIP kit from Cell Signaling Technology with an IP grade DPF2 antibody (Bethyl Laboratories). After reverse cross-link and purification, the associated DNA was subjected to qRT-PCR to detect specific DNA sequences in the pre-miR-223 promoter region. The primers specific to regions 4 and 5 of the pre-miR-223 promoter region were previously reported in Vu et al. (6). Quantitative results are represented as percentages relative to 10% DNA input.

Illustration and Figures. The sequence alignment of DPF2 was generated using ClustalX2 (7) and colored with Alscript (8). Figures were generated using PyMOL (www.pymol.org). Electrostatic potential was calculated with Adaptive Poisson-Boltzmann Solver software (9). The protein interaction network for DPF2 was generated using Cytoscape.

1. Moffat J, et al. (2006) A lentiviral RNAi library for human and mouse genes applied to an arrayed viral high-content screen. *Cell* 124:1283–1298.
2. Kabsch W (2010) XDS. *Acta Crystallogr D Biol Crystallogr* 66:125–132.
3. Adams PD, et al. (2010) PHENIX: A comprehensive Python-based system for macromolecular structure solution. *Acta Crystallogr D Biol Crystallogr* 66:213–221.
4. Emsley P, Cowtan K (2004) Coot: Model-building tools for molecular graphics. *Acta Crystallogr D Biol Crystallogr* 60:2126–2132.
5. Davis IW, et al. (2007) MolProbity: All-atom contacts and structure validation for proteins and nucleic acids. *Nucleic Acids Res* 35:W375–W383.
6. Vu LP, et al. (2013) PRMT4 blocks myeloid differentiation by assembling a methyl-RUNX1-dependent repressor complex. *Cell Reports* 5:1625–1638.
7. Jeanmougin F, Thompson JD, Gouy M, Higgins DG, Gibson TJ (1998) Multiple sequence alignment with Clustal X. *Trends Biochem Sci* 23:403–405.
8. Barton GJ (1993) ALSCRIPT: A tool to format multiple sequence alignments. *Protein Eng* 6:37–40.
9. Baker NA, Sept D, Joseph S, Holst MJ, McCammon JA (2001) Electrostatics of nanosystems: Application to microtubules and the ribosome. *Proc Natl Acad Sci USA* 98: 10037–10041.

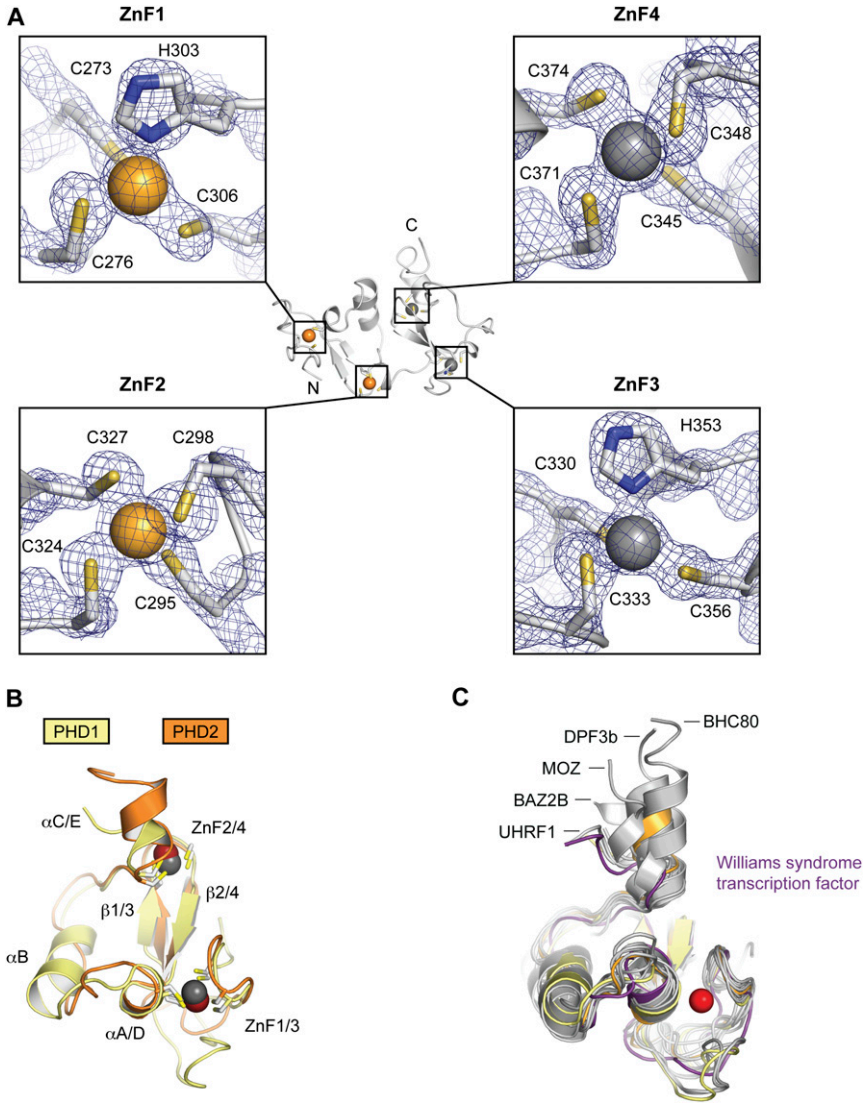

Fig. S1. Structural analysis of human DPF2^{PHD}. (*A*) Final $2|F_O|-|F_C|$ electron density map countered at 1.0 σ around a stick representation of the Zn^{2+} coordinating residues of DPF2^{PHD1} (*Left*) and DPF2^{PHD2} (*Right*). The Zn^{2+} atoms are shown as orange (PHD1) and gray (PHD2) spheres, respectively. (*B*) Superposition of DPF2^{PHD1} and DPF2^{PHD2}, colored as in Fig. 1. (*C*) Superposition of the DPF2^{PHD1} and DPF2^{PHD2}, colored as in Fig. 1, along with representative PHD domains (PDB ID codes 2KWJ, 2PUY, 3SOU, 4LK9, 4L7X, 4QF3) (1–7), all colored in gray.

1. Zeng L, et al. (2010) Mechanism and regulation of acetylated histone binding by the tandem PHD finger of DPF3b. *Nature* 466:258–262.
2. Dreveny I, et al. (2014) The double PHD finger domain of MOZ/MYST3 induces α-helical structure of the histone H3 tail to facilitate acetylation and methylation sampling and modification. *Nucleic Acids Res* 42:822–835.
3. Gatchalian J, et al. (2013) Dido3 PHD modulates cell differentiation and division. *Cell Reports* 4:148–158.
4. Li H, et al. (2006) Molecular basis for site-specific read-out of histone H3K4me3 by the BPTF PHD finger of NURF. *Nature* 442:91–95.
5. Rajakumara E, et al. (2011) PHD finger recognition of unmodified histone H3R2 links UHRF1 to regulation of euchromatic gene expression. *Mol Cell* 43:275–284.
6. Tallant C, et al. (2015) Molecular basis of histone tail recognition by human TIP5 PHD finger and bromodomain of the chromatin remodeling complex NoRC. *Structure* 23:80–92.
7. Lan F, et al. (2007) Recognition of unmethylated histone H3 lysine 4 links BHC80 to LSD1-mediated gene repression. *Nature* 448:718–722.

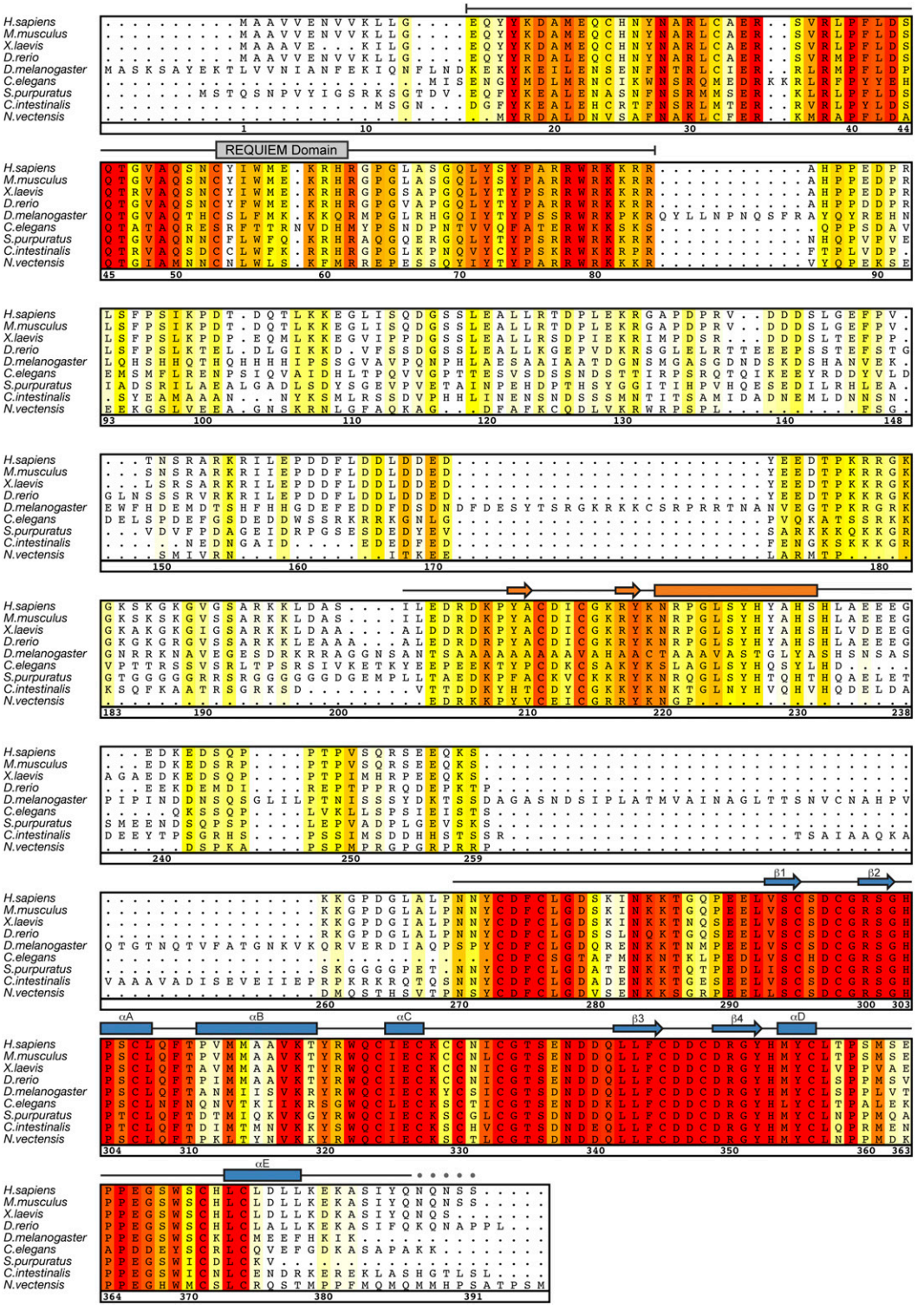

Fig. S2. Multispecies sequence alignment of DPF2 homologs. The secondary structure is indicated above the sequence as cylinders (α-helices), arrows (β-sheets), and lines (coil regions). The numbering below the alignment is relative to human DPF2. Overall sequence conservation at each position is shaded in a color gradient from white (below 40% identity) to yellow (60% identity) to dark red (100% identity). The secondary structure elements above the tandem PHD finger domain (residues 270–391) are as observed in the structure presented here and colored in blue, those above the C2H2 zinc finger domain (residues 206–232) are from the previously solved structure (PDB ID code 3IUF) (1) and colored in orange.

1. Zhang W, et al. (2011) Crystal structure of the Cys2His2-type zinc finger domain of human DPF2. *Biochem Biophys Res Commun* 413:58–61.

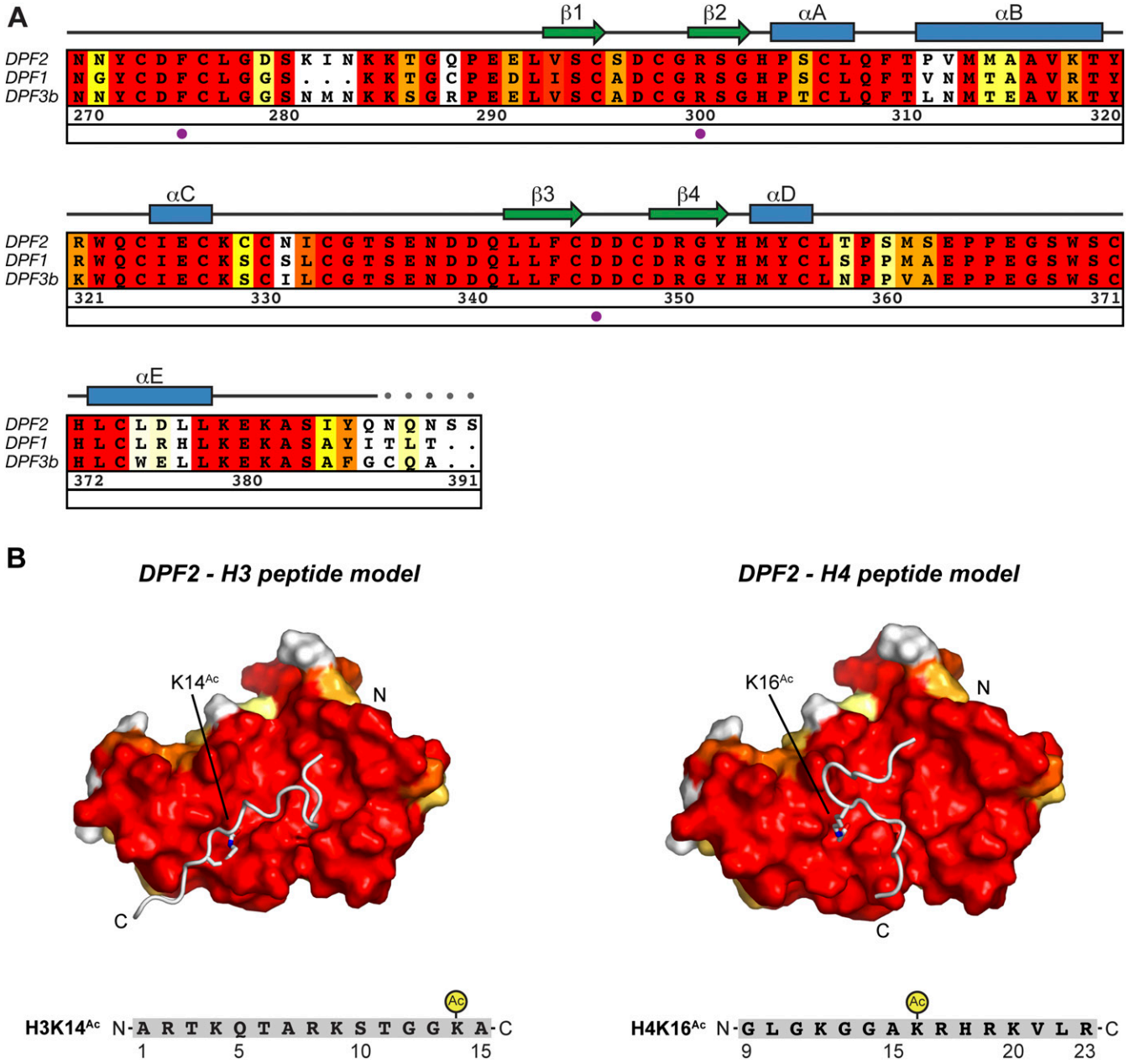

Fig. S3. Sequence alignment of human d4 family members. (*A*) The secondary structure is indicated above the sequence as blue cylinders (α-helices), green arrows (β-sheets), and gray lines (coil regions). The numbering below the alignment is relative to human DPF2. Overall sequence conservation at each position is shaded in a color gradient from white (below 40% similarity) to yellow (60% similarity) to dark red (100% identity). Purple dots indicate residues mutated in our biochemical analysis and gray dots indicate residues for which there was no observed electron density. (*B*) Surface representation of a model of $DPF2^{PHD}$ in complex with the indicated histone peptides based on the DPF3b solution structures (PDB ID codes 2KWJ and 2KWN) (1). The model is colored according to the above multispecies sequence alignment.

1. Zeng L, et al. (2010) Mechanism and regulation of acetylated histone binding by the tandem PHD finger of DPF3b. *Nature* 466:258–262.

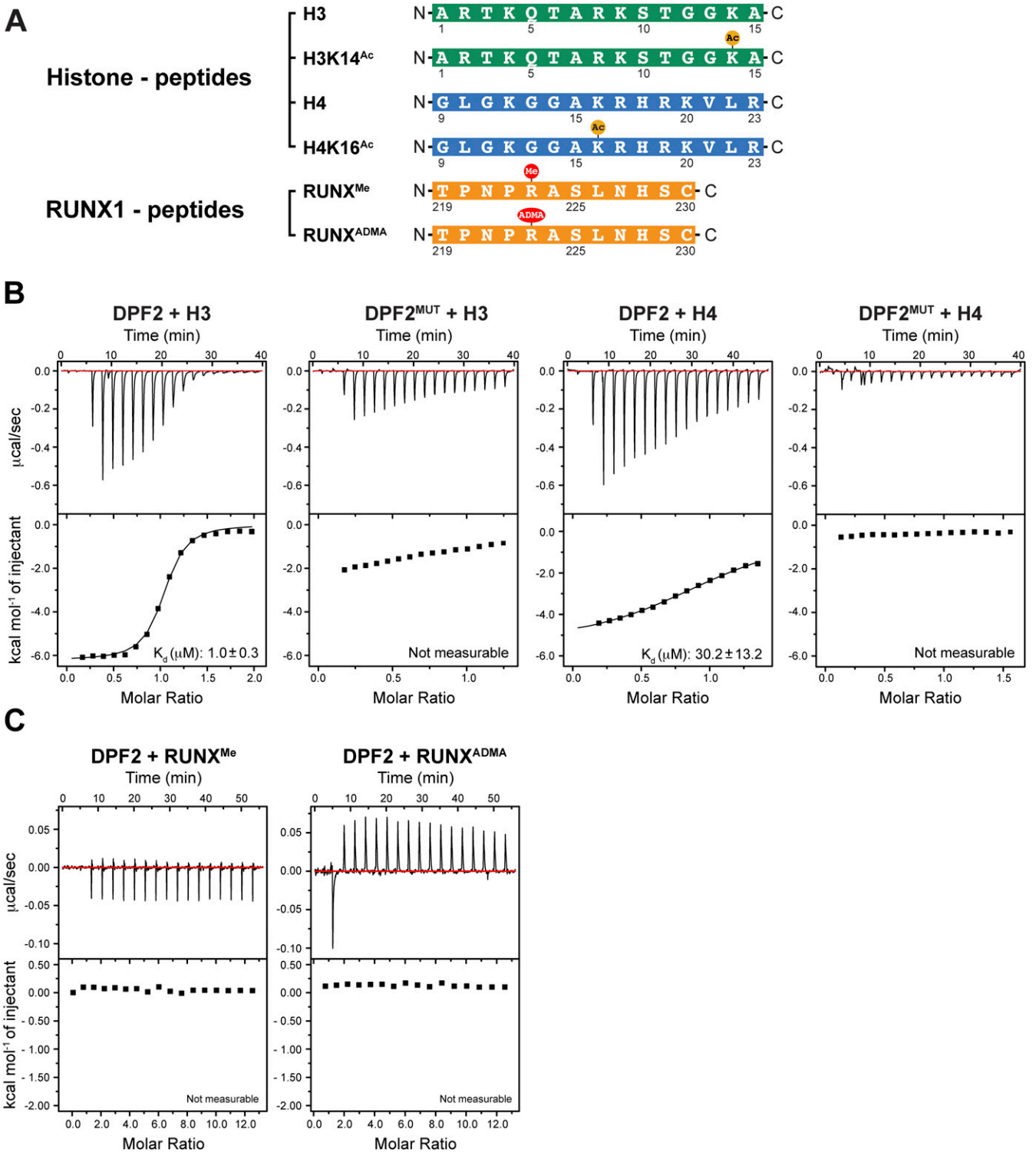

Fig. S4. Biochemical interaction analysis. (*A*) Sequences and modifications of peptides used in interaction experiments (*B*) Representative ITC data for interactions between wildtype DPF2 or a triple mutant (DPF2^{MUT}; F275A, R300A, and D346A) and H3 or H4 histone tail peptides at 100 mM NaCl concentration. *Upper* parts of each box show raw data and *Lower* parts show integrated heat changes corrected for heat from dilution. See also Table S3. (*C*) Representative ITC data for interactions between RUNX1 peptides and DPF2 at 0 mM NaCl concentration. *Upper* parts of each box show raw data and *Lower* parts show integrated heat changes corrected for heat from dilution. See also Table 1.

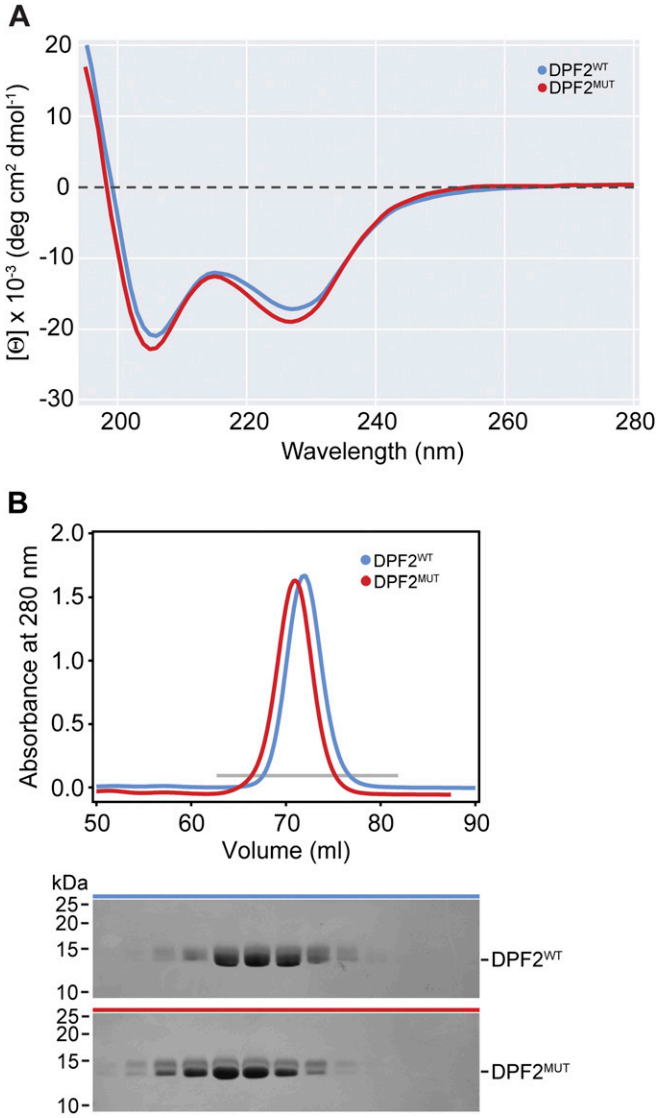

Fig. S5. CD spectroscopy. (*A*) CD spectra of DPF2 wild-type ($DPF2^{WT}$, blue) and a triple mutant ($DPF2^{MUT}$; F275A, R300A, and D346A, red). Spectra were measured in triplicate at a protein concentration of 0.25 mg/mL at 25 °C. (*B*) Size-exclusion chromatography analysis of DPF2 wild-type ($DPF2^{WT}$, blue) and a triple mutant ($DPF2^{MUT}$; F275A, R300A, and D346A, red).

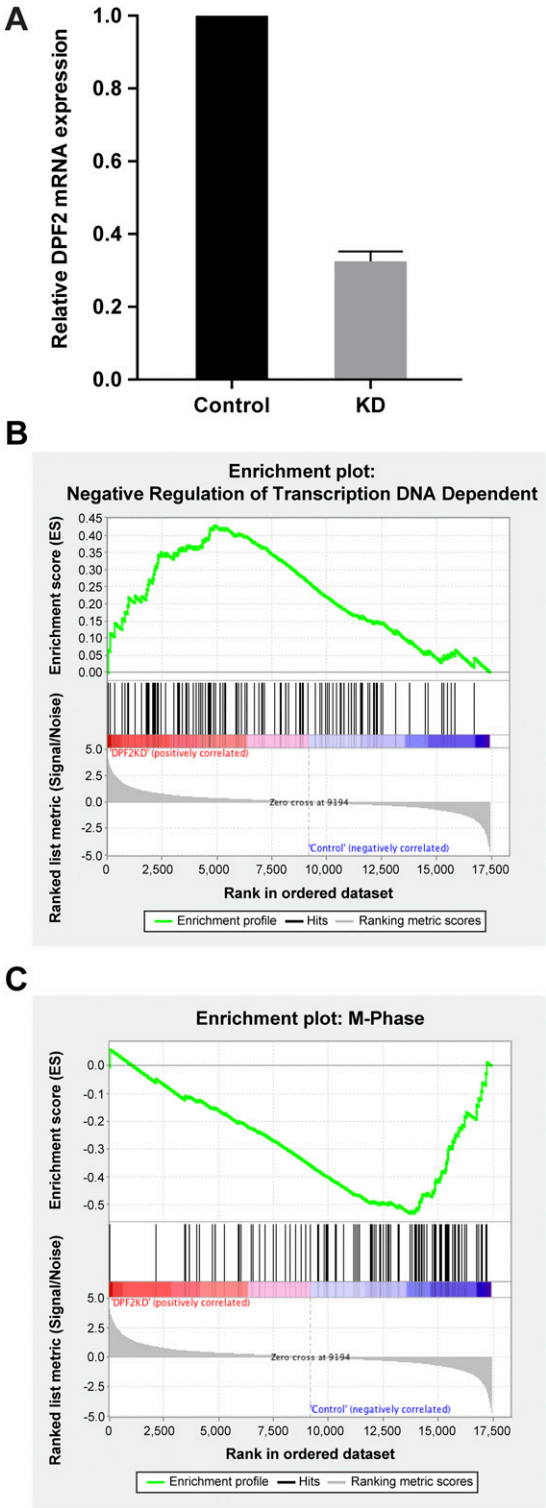

Fig. S6. RNA sequencing reveals a biological role for DPF2 in HSPCs. RNA sequencing of CB CD34^{+} cells expressing DPF2 directed or scrambled control shRNAs was performed 72 h after lentiviral transduction. (*A*) DPF2 KD efficiency determined by relative DPF2 mRNA expression. (*B*) Functional annotation of RNA sequencing analysis by performing GSEA. Representation GSEA plot is shown for datasets with a positive correlation with DPF2 KD. (*C*) Functional annotation of RNA sequencing analysis by performing GSEA. Representation GSEA plot is shown for datasets with a negative correlation with DPF2 KD.

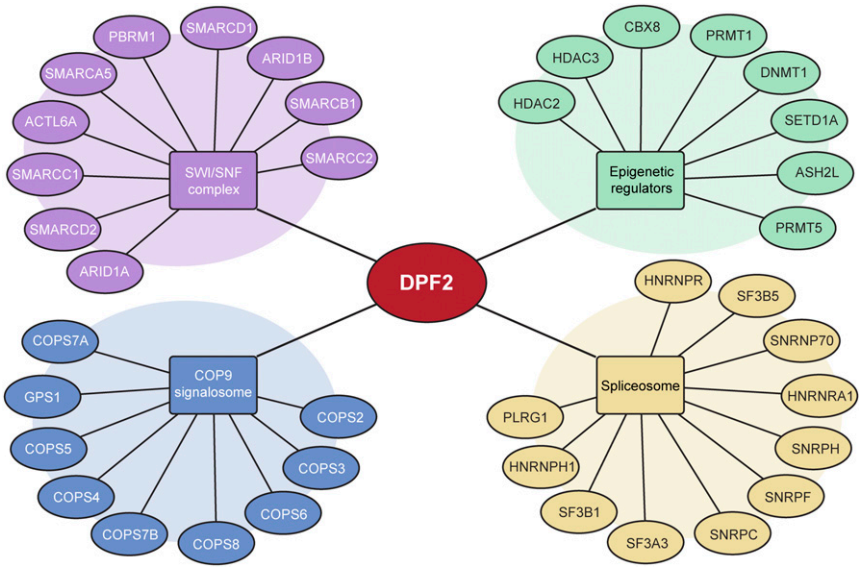

Fig. S7. Schematic representation of the DPF2 interaction network. Endogenous DPF2 was immunoprecipitated from two leukemia cell lines and analyzed by mass spectrometry. Overlapping DPF2 interaction partners from both cell lines include components of the SWI/SNF complex, COP9 signalosome, spliceosomal complex, and epigenetic regulators. See also Table S8.

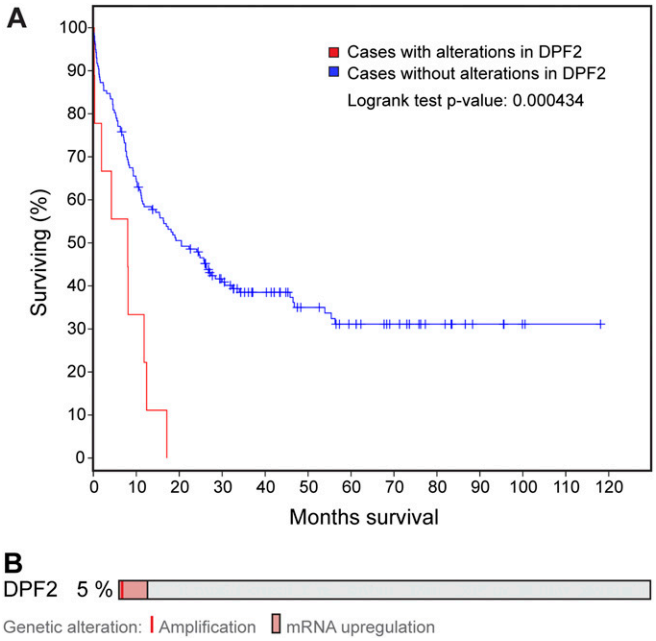

Fig. S8. Analysis of the Cancer Genome Atlas database. (*A*) Overall AML patient survival rates are plotted for de novo AML cases without alterations in the DPF2 gene, represented by the blue line, compared with cases with alterations in the DPF2 gene, represented by the red line. (*B*) Schematic visualizes the 5% of de novo AML patients that display alterations in DPF2. Patient data and graphs retrieved and adapted from the cBio Portal for cancer genomics (1, 2).

1. Cerami E, et al. (2012) The cBio cancer genomics portal: An open platform for exploring multidimensional cancer genomics data. *Cancer Discov* 2:401–404.
2. Gao J, et al. (2013) Integrative analysis of complex cancer genomics and clinical profiles using the cBioPortal. *Sci Signal* 6:pl1.

Table S1. Bacterial expression constructs

Protein	Residues (mutations)	Expression vector	Restriction sites 5′, 3′	N-terminal overhang
*hs*DPF2*	270–391	pGEX-6P-1	BamHI, NotI	Gly-Met-Gly-Ser
*hs*DPF2	270–391 (F275A R300A D346A)	pGEX-6P-1	BamHI, NotI	Gly-Met-Gly-Ser

*Construct that was used for crystallization of *hs*DPF2$^{270–391}$.

Table S2. Crystallographic analysis

Data collection		
Protein	$DPF2^{PHD}$	$DPF2^{PHD}$
PDB ID code		5VDC
Synchrotron	SSRL	SSRL
Beamline	BL12-2	BL12-2
Space group	I422	I422
Cell dimensions		
a, *b*, *c* (Å)	$a = 107.1$, $b = 107.1$, $c = 52.9$	$a = 107.5$, $b = 107.5$, $c = 53.3$
α, β, γ (°)	$\alpha = 90.0$, $\beta = 90.0$, $\gamma = 90.0$	$\alpha = 90.0$, $\beta = 90.0$, $\gamma = 90.0$
	Zn peak	
Wavelength (Å)	1.2818	0.9795
Resolution (Å)	50–1.8	50–1.6
R_{meas} (%)*	6.1 (95.9)	6.9 (171.5)
R_{pim} (%)*	1.3 (16.2)	1.3 (38.8)
$\langle I \rangle / \langle \sigma I \rangle$*	33.0 (3.2)	28.9 (2.2)
$CC_{1/2}$*	100.0 (89.7)	100 (77.8)
Completeness (%)*	100.0 (99.9)	99.0 (98.3)
No. of observations	604,981	540,122
No. of unique reflections*	27,282 (4,408)	20,713 (3,249)
Redundancy*	22.2 (21.9)	26.1 (26.9)
Refinement		
Resolution (Å)		50–1.6
No. of reflections		20,405
No. of reflections test set		1,018
R_{work}/R_{free} (%)		14.6/18.7
No. atoms (nonhydrogen)		1,106
Protein		1,003
Ligand/Ions		16
Water		87
B-factors		38
Protein		37
Ligand/Ions		61
Water		51
Rmsd		
Bond lengths (Å)		0.008
Bond angles (°)		1.2
Ramachandran plot†		
Favored (%)		97.6
Additionally allowed (%)		2.4
Outliers (%)		0.0
MolProbity score†		1.25

*Highest-resolution shell is shown in parentheses.
†As determined by MolProbity (1).

1. Davis IW, et al. (2007) MolProbity: All-atom contacts and structure validation for proteins and nucleic acids. *Nucleic Acids Res* 35:W375–W383.

Table S3. Isothermal titratrion calorimetry measurements

Protein	Peptide	Salt concentration (mM)	K_d (μM)	ΔH (kcal/mol)	ΔS (cal/mol/deg)
DPF2^{WT}	H3	No salt	0.05 ± 0.02	−6.2 ± 0.4	12.5
		50	0.2 ± 0.1	−6.7 ± 0.7	8.2
		100	1.0 ± 0.3	−6.2 ± 0.2	6.8
	H3K14^{Ac}	No salt	0.04 ± 0.02	−10.2 ± 0.5	0.1
		50	0.2 ± 0.02	−9.7 ± 0.1	−2.3
		100	1.1 ± 0.4	−9.7 ± 0.2	−5.3
	H4	No salt	0.2 ± 0.04	−6.7 ± 0.3	8.0
		50	3.9 ± 1.5	−7.0 ± 0.1	1.4
		100	30.2 ± 13.2	−6.3 ± 0.7	−0.2
	H4K16^{Ac}	No salt	0.6 ± 0.3	−8.9 ± 6.7	−1.1
		50	6.8 ± 1.0	−10.7 ± 0.5	−12.0
		100	50.4 ± 5.7	−9.0 ± 0.5	−10.5
	RUNX1R223^{Me}	No salt	Not measurable	Not measurable	Not measurable
	RUNX1R223^{ADMA}	No salt	Not measurable	Not measurable	Not measurable
DPF2^{MUT}	H3	50	24.8 ± 4.8	−5.1 ± 0.3	4.1
		100	Not measurable	Not measurable	Not measurable
	H3K14^{Ac}	No salt	2.8 ± 0.1	−6.0 ± 0.2	5.4
		50	39.5 ± 13.0	−5.3 ± 0.5	2.4
		100	Not measurable	Not measurable	Not measurable
	H4	50	16.4 ± 1.3	−3.1 ± 0.3	11.6
		100	Not measurable	Not measurable	Not measurable
	H4K16^{Ac}	No salt	3.4 ± 0.2	−4.9 ± 0.3	8.7
		50	48.1 ± 9.7	−3.7 ± 0.3	7.4
		100	Not measurable	Not measurable	Not measurable
DPF3b*	H3	50	2.3 ± 0.7	−4.4 ± 0.2	11.1
	H3K14^{Ac}	50	0.5 ± 0.1	−6.6 ± 0.1	6.7
	H4	50	28.8 ± 7.8	−3.3 ± 0.4	9.7
	H4K16^{Ac}	50	46.9 ± 10.0	−4.6 ± 0.6	4.4

*Data reported in Zeng et al. (1).

1. Zeng L, et al. (2010) Mechanism and regulation of acetylated histone binding by the tandem PHD finger of DPF3b. *Nature* 466:258–262.

Table S4. Mammalian expression constructs

Protein	Residues (mutations)/target sequence	Expression vector	Restriction sites 5′, 3′	Source
*hs*DPF2	1–391	pCDH-EF1-MCS-(PGK-GFP)	BamHI	Present study
*hs*DPF2	1–391 (F275A R300A D346A)	pCDH-EF1-MCS-(PGK-GFP)	BamHI	Present study
*hs*DPF2^{PHD}	270–391	pCDH-EF1-MCS-(PGK-GFP)	BamHI	Present study
FLAG-*hs*DPF2	1–391	pCDNA3.1-FLAG	EcoRI, NotI	Present study
FLAG-*hs*DPF2	1–391 (F275A R300A D346A)	pCDNA3.1-FLAG	EcoRI, NotI	Present study
*hs*DPF2 shRNA	CCAGGCCTCAGTTACCACTAT	pLKO.1-U6-(PGK-GFP)	EcoRI, AgeI	Present study
Control shRNA	GGAATCTCATTCGATGCATAC	pLKO.1-U6-(PGK-GFP)	EcoRI, AgeI	Present study
FLAG-*hs*RUNX1c	1–480	pBGJR-EF1-(PGK-GFP)	RsrII	Vu et al. (1)

1. Vu LP, et al. (2013) PRMT4 blocks myeloid differentiation by assembling a methyl-RUNX1-dependent repressor complex. *Cell Reports* 5:1625–1638.

Table S5. Significant GO-terms enriched in the DPF2 KD dataset

GO term-enriched DPF2 KD vs. Control (438 genes)	*P* value
Regulation of transcription, DNA-templated (GO:0006355)	4.63E-06
Regulation of metabolic process (GO:0019222)	5.51E-06
Regulation of cellular biosynthetic process (GO:0031326)	6.67E-06
Regulation of macromolecular biosynthetic process (GO:0010556)	7.46E-06
Regulation of RNA biosynthetic process (GO:2001141)	7.58E-06
Regulation of nucleic acid-templated transcription (GO:1903506)	8.28E-06
Regulation of gene expression (GO:0010468)	8.39E-06
Regulation of RNA metabolic process (GO:0051252)	1.43E-05
Transcription, DNA-templated (GO:0006351)	1.56E-05
Nucleic acid-templated transcription (GO:0097659)	1.60E-05
M-phase (GO:0000279)	4.20E-02

Results for the significant GO-terms enriched in the DPF2-KD data set compared with the control and analyzed by the GO and PANTHER classification system.

Table S6. Enriched genes for "negative regulation of transcription DNA dependent" with positive correlation to DPF2 KD

Sample	Description
GLIS1	GLIS1 family zinc finger 1
ZNF177	Zinc finger protein 177
NR0B1	Nuclear receptor subfamily 0, group B, member 1
NKX2-5	NK2 transcription factor related, locus 5 (*Drosophila*)
ZBTB32	Zinc finger and BTB domain containing 32
SMAD3	SMAD, mothers against DPP homolog3 (*Drosophila*)
BMP2	Bone morphogenetic protein 2
SIRT4	Sirtuin (silent mating type information regulation 2 homolog) 4 (*Saccharomyces cerevisiae*)
TGIF1	TGIFB induced factor homeobox 1
RYBP	RING1 and YY1 binding protein
ZBTB16	Zinc finger and BTB domain containing 16
GLI2	GLI-Kruppel family member GLI2
POU4F2	POU domain, class4, transcription factor 2
MDM2	Mdm2, transformed 3T3 cell double minute 2, p53 binding protein (mouse)
DRAP1	DR1-associated protein 1 (negative cofactor 2α)
KDM5B	Lysine demethylase 5B
ZNF345	Zinc finger protein 345
ZEB1	Zinc finger E-box binding homeobox 1
HDAC5	Histone deacetylase 5
CIR1	Corepressor interacting with RBPJ,1
KLF11	Kruppel-like factor 11
ARID5B	AT rich interactive domain 5B (MRF1-like)
NR6A1	Nuclear receptor subfamily 6, group A, member 1
KLF4	Kruppel-like factor 4
TWIST1	Twist homolog 1 (acrocephalosyndactyly 3; Saethre-Chotzen syndrome) (*Drosophila*)
ARID5A	AT rich interactive domain 5A (MRF1-like)
FST	Follistatin
MXD4	MAX dimerization protein 4
TBX3	T-box 3 (ulnar mammary syndrome)
SLA2	Src-like-adaptor 2
VHL	Von Hippel-Lindau tumor suppressor
JAZF1	JAZF zinc finger 1
RSF1	Remodeling and spacing factor 1
ZNF189	Zinc finger protein 189
PEX14	Peroxisomal biogenesis factor 14
E2F6	E2F transcription factor 6
EID1	EP300 interacting inhibitor of differentiation 1
EPC1	Enhancer of polycomb homolog 1 (*Drosophila*)
FOXN3	Forkhead box N3
PHF21A	PHD finger protein 21A
CBY1	Chibby homolog 1 (*Drosophila*)
STAT3	Signal transducer and activator of transcription 3 (acute-phase response factor)
SIRT1	Sirtuin (silent mating type information regulation 2 homolog) 1 (*S. cerevisiae*)
IRF8	IFN regulatory factor 8
FOSB	FBJ murine osteosarcoma viral oncogene homolog B
TP63	Tumor protein P63
ZNF238	Zinc finger protein 238
ZNF136	Zinc finger protein 136
ZHX2	Zinc fingers and homeoboxes 2
SUPT5H	Suppressor of TY 5 homolog (*S. cerevisiae*)
MDM4	Mdm4, transformed 3T3 cell double minute 4, p53 binding protein (mouse)
VPS72	Vacuolar protein sorting 72 (*S. cerevisiae*)
ZNF281	Zinc finger protein 281
BPTF	Bromodomain PHD finger transcription factor
PPARD	Peroxisome proliferative activated receptor, δ
IRF7	IFN regulatory factor 7
NRIP1	Nuclear receptor interacting protein 1
ZMYND11	Zinc finger, MYND domain containing 11
ZNF202	Zinc finger protein 202
SPI1	Spleen focus forming virus (SFFV) proviral integration oncogene spi1
HDAC8	Histone deacetylase 8
ARID4A	AT rich interactive domain 4A, (RBP1-like)

Table S6. Cont.

Sample	Description
SUPT4H1	Suppressor of Ty 4 homolog 1 (*S. cerevisiae*)
ZNF174	Zinc finger protein 174
MEIS2	Meis1, myeloid ecotropic viral integration site 1 homolog 2 (mouse)
ZHX1	Zinc fingers and homeoboxes 1
ZNF148	Zinc finger protein 148
SMAD4	SMAD, mothers against DPP homolog 4 (*Drosophila*)
ZFP161	Zinc finger protein 161 homolog (mouse)
NFX1	Nuclear transcription factor, X-box binding 1
HSBP1	Heat-shock factor binding protein 1
NDUFA13	NADH dehydrogenase (ubiquinone) 1 alpha subcomplex, 13
NR0B2	Nuclear receptor subfamily 0, group B, member 2
MECP2	Methyl CpG binding protein 2 (Rett syndrome)
SMARC22	SWI/SNF related, matrix associated, actin dependent regulator of chromatin, subfamily c, member 2
SIRT5	Sirtuin (silent mating type information regulation 2 homolog) 5 (*S. cerevisiae*)
GLIS3	GLIS family zinc finger 3
TBX2	T-box 2
SMAD2	SMAD, mothers against DPP homolog 2 (*Drosophila*)

Table S7. Enriched genes for "negative regulation of transcription DNA dependent" with negative correlation to DPF2 KD

Sample	Description
SMARCE1	SWI/SNF related, matrix associated, actin dependent regulator of chromatin, subfamily e, member 1
SIN3A	SIN3 homolog A, transcription regulator (yeast)
FOXP3	Forkhead box P3
CTCF	CCCTC-binding factor (zinc finger protein)
CUX1	Cut like Homeobox 1
DAXX	Death-associated protein 6
MEN1	Multiple endocrine neoplasia I
RB1	Retinoblastoma 1 (including osteosarcoma)
KLF12	Kruppel-like factor 12
LDB1	LIM domain binding 1
NSD1	Nuclear receptor binding SET domain protein 1
E2F1	E2F transcription factor 1
RBPJ	Recombination signal binding protein for Ig κ J
CSDA	Cold shock domain protein A
MDFI	MyoD family inhibitor
TRIM27	Tripartite motif-containing 27
PAWR	PRKC, apoptosis, WT1, regulator
ZNF254	Zinc finger protein 254
FOXD3	Forkhead box D3
BCOR	BCL6 corepressor
PRDM1	PR domain containing 1, with ZNF domain
ENO1	Enolase 1, (α)
KLF10	Kruppel-like factor 10
ATF7IP	Activating transcription factor 7 interacting protein
PHF12	PHD finger protein 12
HEXIM2	Hexamethylene bis-acetamide inducible 2
CHMP1A	Chromatin modifying protein 1A
ORC2	Origin recognition complex subunit 2
ZNF396	Zinc finger protein 396
DR1	Down-regulator of transcription 1, TBP-binding (negative cofactor 2)
ZNF593	Zinc finger protein 593
PA2G4	Proliferation-associated 2G4, 38 kDa
GATAD2A	GATA zinc finger domain containing 2A
ILF3	Interleukin enhancer binding factor 3, 90 kDa
DNMT1	DNA (cytosine-5-)-methyltransferase
HEXIM1	Hexamethylene bis-acetamide inducible 1
BCL6	B-cell CLL/lymphoma 6 (zinc finger protein 51)
GFI1B	Growth factor independent 1B (potential regulator of CDKN1A, translocated in CML)
IRF2	IFN regulatory factor 2
ZNF157	Zinc finger protein 157
TCEAL1	Transcription elongation factor A (SII)-like 1
HMGB1	High-mobility group box 1

Table S8. RUNX1 and DPF2 interaction partners

Methyl RUNX1 Interaction partners		DPF2 Interaction partners		
ACTB	MED16	ACAD9	ETFA	NSRP1
ARID1A	MED17	ACLY	FAM102B	NSUN4
ARID3A	MED26	ACOT13	FAM120A	NXN
ASH2L	MEN1	ACTL6A	FAM133A	OLA1
BAF53a	MLLT1	ACTR5	FAM32A	PAPOLG
BRD9	MTA2	AIMP1	FAM76B	PCCB
C2orf44	NDC80	AIMP2	FOXK1	PDIA6
CBFA2T3	NOL5A	ARF1	FUBP3	PHAX
CCNK	NONO	ARF4	GATAD2A	PIP
CDC16	NUP85	ARID1B	GFPT1	PKMYT1
CDKN2AIP	ORC2L	ARPC1B	GMFB	PLOD3
CLTC	PABPC1	ASH2L	GPATCH8	PLRG1
COBRA1	PABPC4	ATP13A1	GPS1	PNISR
CPSF3	PAXIP1	ATP2A1	H1F0	POLR1C
CPSF6	PRMT5	ATP2A2	HBB	POLR1D
CSTF2	PSIP1	ATP5C1	HBG1	POLR2C
CSTF2T	PSPC1	ATXN2L	HDAC2	POLR2E
CTPS	RAD18	BCR	HIST1H1D	POLR3D
DDX1	RANGAP1	BRD9	HIST1H1E	PPIL4
DDX17	RARS	BRIX1	HIST1H2AD	PPP1CA
DDX21	RBBP5	BRPF3	HMGXB4	PPP2CA
DDX3X	RBM14	CALML3	HNRNPAB	PRKCB
DDX41	RBM39	CAPN1	HNRNPR	PRMT1
DDX5	RPA1	CAPZA1	HSP90AA2	PRPH
DHX15	RPAP2	CARS	HSP90B1	PRSS3
DHX36	SF1	CBX8	HSP90B2P	PSMA1
DHX9	SF3B2	CCDC59	IMMT	PSMC6
DPF2	SF3B3	CCNT1	IMP4	PSPC1
EEF1A1	SFPQ	CDC16	INA	PTBP3
EEF1A2	SMARCA4	CDK18	KIF26A	PTPRE
EWSR1	SMARCC1	CDK9	KLC4	RAB6A
EZR	SMARCC2	CEP112	LARP1	RAP1A
FAF1	SMARCD1	CEP170	LASP1	RAP2B
FERMT3	SNRNP70	CHID1	LCP1	RBM14
FIP1L1	SNRPD1	CHMP4B	LIN28B	RPA1
FUBP1	SNX9	CIRBP	LRRC59	RPA2
FUS	SR140	CIRH1A	LUC7L3	RPL26
GATAD2A	SRP68	CLTA	MAZ	RPLP2
GATAD2B	SYNCRIP	CMAS	MCM3	SCYL2
GMPS	TAF15	COPS3	MCM6	SF3B1
HIC2	TCF3	COPS4	MED16	SF3B5
HNRNPH1	TFRC	COPS5	METAP2	SMARCA4
HNRNPM	TKT	COPS6	MRM1	SMARCA5
HNRNPR	TRAP1	COPS7A	MRPL13	SMARCB1
HNRNPU	TRIM25	COPS7B	MRPL19	SMARCC1
HSPA1A	TUBA1B	COPS8	MRPL23	SMARCC2
HSPA2	TUBB2A	CPSF7	MRPL27	SMARCD1
HSPA5	UBP1	DBT	MRPL38	SMARCD2
HSPA8	USP39	DCAF13	MRPL4	SNRNP70
HSPA9	WDR76	DDX1	MRPL43	TAGLN2
IGF2BP1	XRCC6	DDX5	MRPL45	TALDO1
INTS10	XRN2	DHFR	MRPS10	TFRC
INTS9	ZNF326	DHX36	MRPS2	TPI1
KHSRP		DMBT1	MRPS22	TUBA1B
KIF2B		DNAJA3	MRPS35	VPS26A
LARP7		DNAJB11	MYL1	WDHD1
LCP1		DNMT1	MYL12A	WDR36
LMNA		DPYSL2	MYL6	WDR74
LMNB1		DYNLL1	NAP1L4	XRN2
LRRC40		EIF3A	NBR1	ZNF326
LRWD1		EIF3G	NEMF	ZNF580
MED1		EIF4A2	NOLC1	
MED12		EMG1	NOP14	

Table S9. Overlapping interaction partners of asymmetric dimethyl-R223 RUNX1 peptide and DPF2

Protein	Description	Molecular function
ASH2L	Member of SWI/SNF complex	Chromatin remodeling, regulation of transcription
BRD9	Bromodomain containing protein 9	Chromatin remodeling, regulation of transcription
CDC16	Cell division cycle 16	Regulation of mitosis
DDX1	DEAD (Asp-Glu-Ala-Asp) box polypeptide 1	Translation initiation, RNA splicing
DDX5	DEAD (Asp-Glu-Ala-Asp) box polypeptide 5	Translation initiation, RNA splicing
DHX36	DEAH (Asp-Glu-Ala-His) box polypeptide 36	Nucleic acid binding, transcription regulation
GATAD2A	GATA zinc finger domain containing 2A	Regulation of transcription
HNRNPR	Heterogeneous nuclear ribonucleoprotein R	Regulation of RNA splicing
LCP1	Lymphocyte cytosolic protein 1 (L-plastin)	Actin filament assembly
MED16	Mediator complex subunit 16	Regulation of transcription
PSPC1	Paraspeckle component 1	Regulation of transcription
RBM14	RNA binding motif protein 14	Regulator of transcription
RPA1	Replication protein A1, 70 kDa	DNA recombination and repair
SMARCA4	Member of SWI/SNF complex	Chromatin remodeling, regulation of transcription
SMARCC1	Member of SWI/SNF complex	Chromatin remodeling, regulation of transcription
SMARCC2	Member of SWI/SNF complex	Chromatin remodeling, regulation of transcription
SMARCD1	Member of SWI/SNF complex	Chromatin remodeling, regulation of transcription
SNRNP70	Small nuclear ribonucleoprotein 70 kDa (U1)	Regulation of RNA splicing
TFRC	Transferrin receptor (p90, CD71)	Cellular iron ion homeostasis, endocytosis
TUBA1B	Tubulin, α1b	Microtubule assembly
XRN2	5′-3′ exoribonuclease 2	Transcription regulation
ZNF326	Zinc finger protein 326	Regulation of transcription